Multidirectional visible and shortwave infrared polarimeter for atmospheric aerosol and cloud observation: OSIRIS (Observing System Including PolaRisation in the Solar Infrared Spectrum)

F. Auriol, J.-F. Léon, J.-Y. Balois, C. Verwaerde, P. François, J. Riedi, F. Parol, F. Waquet, D. Tanré, P. Goloub

Multidirectional visible and shortwave infrared polarimeter for atmospheric aerosol and cloud observation: OSIRIS (Observing System Including PolaRisation in the Solar Infrared Spectrum)

Auriol, F.*, J.-F. Léon, J.-Y. Balois, C. Verwaerde, P. François, J. Riedi, F. Parol, F. Waquet, D. Tanré and P. Goloub
Laboratoire d'Optique Atmosphérique, CNRS – Université de Lille 1, Villeneuve d'Ascq, France

ABSTRACT

The aim of this project is to improve the characterization of radiative and microphysical properties of aerosols and clouds in the atmosphere. These two atmospheric components and their interactions are among the main sources of uncertainty in the numerical forecast of climate change. In this context, we have designed a new airborne polarimeter for measuring directional, total and polarized radiances in the 440 to 2200 nm spectral range. This instrument is based on the POLDER concept, instrument that is currently aboard the PARASOL microsatellite. This new sensor consists in two optical systems for the visible to near infrared range (440 to 940 nm) and the shortwave infrared (940 to 2200 nm). Each optical system is composed of a wide field-of-view optics (114° and 105° respectively) associated to two rotating wheels for interferential filters and analysers respectively, and a 2D array of detectors. For each channel, the total and polarized radiances are computed using the measurements performed with the three analysers shifted by an angle of 60°. Thanks to the large field of view of the optics, any target is seen under several viewing angles during the aircraft motion. This type of instrument has been designed for the retrieval of optical thickness and microphysical properties of aerosols as well as for the determination of microphysical, macrophysical and radiative properties of clouds. In this paper, we will present this new instrument design and some preliminary results recently obtained during the first field campaign in May 2008 over Europe.

Keywords: aerosols, clouds, airborne imaging radio-polarimeter, visible and shortwave infrared, multi-angularity

1. INTRODUCTION

Aerosol particles in the atmosphere can affect the radiation balance of the earth-atmosphere system by reflecting and absorbing sunlight and absorbing and emitting infrared radiation. Moreover, aerosols play a crucial role in the life cycle and optical properties of clouds. Climate change estimations consider both a direct effect of aerosols on radiation budget and an indirect effect through the interaction with clouds. Current estimation of the magnitude and sign of the aerosol impact on climate is still an issue because of large remaining uncertainties [1]. A major uncertainty in the determination of this sensitivity is the misunderstanding in the feedbacks associated with cloudiness changes and the difficulty of GCMs to correctly account for cloud-radiation-climate interactions [2,4]. Indeed cloud-radiation interactions are really complex and depend on numerous physical parameters such as the cloud macrophysical and microphysical characteristics but also the atmospheric and terrestrial environment. Consequently, GCMs need realistic representation of clouds and their effects on radiation balance at global scale as well as at regional scale. It is essential to correctly simulate the present forcing of clouds on radiation but especially to model what the future forcing of clouds will be. Global observations of cloud properties and global measurements of the effects of clouds on radiation are essential to achieve this objective.

Multispectral, Hyperspectral, and Ultraspectral Remote Sensing Technology, Techniques, and Applications II, edited by Allen M. Larar, Mervyn J. Lynch, Makoto Suzuki, Proc. of SPIE Vol. 7149, 71491D
 · doi: 10.1117/12.806421

During the last decade, the development of space borne remote sensing has provided a considerable amount of observations on aerosol load and properties at the global scale [5, 6]. Space borne radiometers make use of the reflected sunlight by the earth-atmosphere system in specific spectral bands to determine the aerosol optical properties. The aerosol optical thickness (or optical depth) is the primary parameter that can be retrieved. Information on the aerosol size distribution can also be derived depending on the spectral capacity of the instruments [7], e.g. the moderate resolution imaging spectroradiometer-MODIS [8] retrieval method is based on the use of spectral channels between 0.4 to 2.2µm [9]. In the shortwave solar infrared (above 1 µm), the effect of submicronic particles on radiance becomes small therefore highlighting the contribution of large supermicronic dust particles. The 2.2 µm channel is then suitable to assess the relative contribution of coarse particle to the aerosol optical depth. However, the retrieval of aerosol parameters depends on the optical properties of the under-laying surface. Indeed, one of the main difficulty in aerosol remote sensing from space in the solar spectrum remains in separating the aerosol contribution from that of the surface [10]. Over ocean, the surface is dark enough in the shortwave spectrum to do not mask the atmospheric signal. Over land surfaces, the albedo strongly depends on the land surface type and vegetation cover. The albedo of dark dense vegetation is low enough to enable the retrieval of aerosol optical thickness [11]. However the surface albedo remains one of the largest uncertainty in the aerosol optical depth retrieval [12].

Polarized measurements provide an alternative and robust approach for the study of aerosols over land. Indeed, the polarized surface contribution is smaller than, or equal to, that of the atmosphere. Moreover, it shows little spectral dependence and generally weak spatial contrast, except for cultivated land and in the transition between urban and natural surfaces [13, 14]. The surface bidirectional polarized distribution function (BPDF) can be modeled using simple mathematical formula based on Fresnel reflection law [13, 15, 16] and even adjusted by using observations of the polarization by the surface [17]. However, using a BPDF model to predict the surface polarized reflectance can introduce significant uncertainties in the retrieval of the aerosol optical thickness. It is therefore desirable to have a direct estimate of the surface polarized reflectance. When considering a large ratio of the wavelength to the size of the particle, the atmosphere tends to be thin and then the surface can be observed. Kaufman et al. [18] have used a channel at 2.2 µm to evaluate the surface reflectance. This estimation is then extrapolated to shorter wavelengths using empirical ratios [19]. With such a method, the accuracy in the retrieved aerosol optical depth remains however lower than for the retrieval over ocean surface [20]. Moreover, the use of fix ratios might not be adequate for all kind of surfaces and especially over urban or peri-urban areas [21, 22]. The main advantage is that the spectral dependence of the surface polarized reflectance is extremely weak over the 0.4-2.2 µm spectral range. It is therefore not necessary to have a fix ratio to extend the 2.2 µm observation of the surface [21].

Launched in 1996, the Polarization and Directionality of Earth's Reflectance (POLDER) was the first instrument that was able to measure the angular distribution of the total and polarized top-of-atmosphere reflected sunlight [23]. The linear degree of polarization is sensitive to the aerosol microphysics and refractive index. Despite the short spectral range (0.44 to 0.94 µm) of POLDER, specific algorithms have been developed to retrieve the total, fine mode fraction, and coarse non-spherical particles optical depth [24] over ocean. Over land, the retrieval is limited to the fine mode fraction of the optical depth [25]. This limitation is caused by the weak sensitivity of the method to the coarse dust particle. The POLDER has flown on the Japanese platform ADEOS-1 (November 96 – June 97), and ADEOS-2 (April – October 2003) and still now on the French micro-satellite PARASOL (data since April 2005). The most important feature of the POLDER is its capacity to measure a given target under several (up to 14) viewing geometries. It provides an estimation of the light scattering pattern of the aerosols which depends on the size, shape, internal structure and refractive index of the particles [26]. The multiangle imaging technique is part of the design of recent sensors dedicated to aerosol remote sensing [27, 28].

One of the weakness of the POLDER is its lack of observations in the SWIR. Recent in lab developments have been undertaken to make a new design of the POLDER that will cover the VIS-NIR and the SWIR spectral range. In this paper, we present a new airborne prototype called the Observing System Including polaRization in the solar Infrared Spectrum (OSIRIS). The primary objectives of this prototype are to validate the POLDER concept in the SWIR and develop the retrieval algorithm for land and ocean aerosol monitoring. We give a detailed presentation of the instrument design and implementation and some very first results of flight campaigns.

2. INSTRUMENT DESIGN

2.1 OSIRIS Instrument

OSIRIS is based on the same imaging radiometer concept as the POLDER [23, 29, 30]. The original concept is composed of a bidimensional CCD matrix, a rotating wheel that carries filters and polarizers, and a wide field of view lens. The OSIRIS has two optical systems: one for the visible and near infrared range (VIS-NIR, from 440 to 940 nm) and the other for the shortwave infrared (SWIR, from 940 to 2200 nm). **Figure 1** summarizes the overall design of the instrument. Each optical system is composed of a wide field-of-view optics (see section 2.4). The field-of-view are 114° and 105° for the VIS-NIR and the SWIR, respectively. Each optics is associated with two rotated wheels for interferential filters and polarizers, respectively. The wheels turn thanks to four step by step motors that move each filter one after the other in front of the detector. Then the imaging system consists in a 2D array of detectors (see section 2.5). The polarizer wheels are also equipped with an opaque shutter for the estimation of the detector dark current.

The size of the instrument is 325x286x188 mm and its weight is 12 kg without his standard four inch PC acquisition rack (17 kg) and the one inch rack-mounted screen for acquisition display (11kg). Total power consumption is 28V-11A (DC).

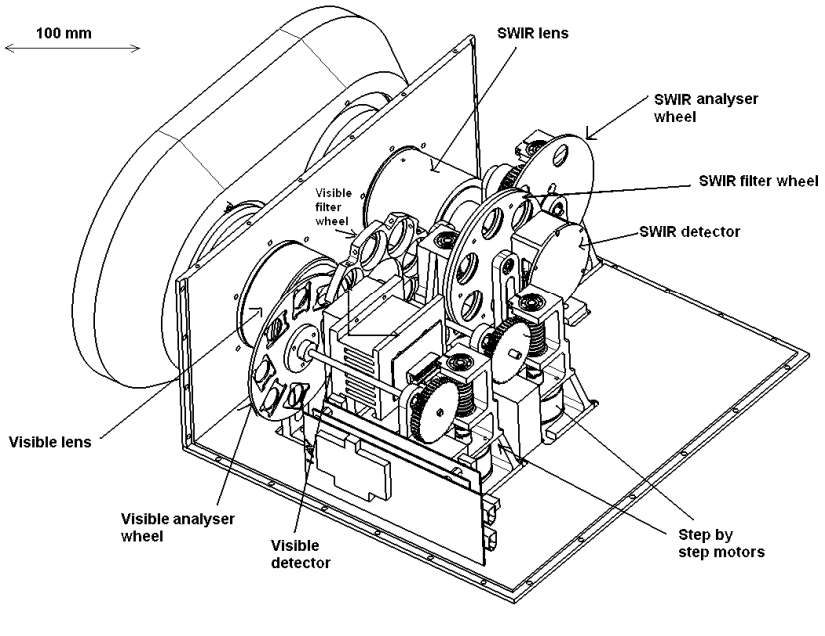

Figure 1. Mechanical scheme of OSIRIS instrument

2.2 Spectral wavelengths

OSIRIS has 8 spectral bands in the VIS-NIR and 6 in the SWIR. **Table 1** gives the position and the full width at half maximum of each of the filters, as well as constructor reference and filter size. In the VIS-NIR (**Figure 2**, left) the first channel is at 440 nm. Another channel is at 490 nm because calibration issues were reported with the 440 nm channel on the POLDER on ADEOS. Those 2 channels are used for aerosol remote sensing. In polarization, the blue channels are highly sensitive to the molecular scattering, while the aerosols tend to mask the polarization by molecules. It is therefore expected to retrieve an index of the mean altitude of the aerosol layer from the polarized blue channels. The 673 and 865 nm channels are extensively used for aerosol remote sensing over land and ocean in total and polarization [24, 25]. The oxygen A-band is covered by one narrow and one large band (see **Figure 2**, left). The reflectance ratio from those two

bands is used to retrieve the altitude of clouds [31]. Tentative retrieval of aerosol scale height has also been proposed [32]. The 2 bands located at 910 and 940 nm are dedicated to the retrieval of water vapor content [33, 34]. VIS-NIR and SWIR have a common channel at 940 nm for inter-calibration purpose.

Regarding cloud studies, the extended spectral range available on OSIRIS will provide valuable information for the following purposes. The first point concerns chiefly the cloud versus snow/ice discrimination based on the difference of spectral behavior : while low-level clouds and snow/ice appear very similar in the visible domain, snow and ice present a rapid decrease in reflectivity in the near infrared. It is worthy of note that, in addition to a window channel, a channel centered on the strong water-vapor absorption at 1.38 μm is very useful for the detection of thin cirrus [35].

For derivation of cloud microphysical properties, comparison of measurements at 1.6 μm - and at 2.2 μm - with visible measurements can be used to infer the cloud particle size [36,38]. This will fill a gap in current POLDER retrieval algorithm. Indeed, a problem in the multi-directional reflectance analysis is related to the sensitivity of the signal to both macrophysical and microphysical cloud properties. Note that the interest of such spectral reflectance measurements is complemented by that of polarization measurements since the cloud particle size can also be deduced from near infrared polarization [39]. Finally, an important point concerns the estimation of the Short Wave cloud forcing. From present multidirectional visible instrument as POLDER, SW reflectances are estimated from narrow band measurements. Infrared cloud reflectance (from ~ 1 to 4 μm) differs notably from reflectance measured in the visible range because of the absorption by water vapor and cloud particles. The water vapor absorption over the whole solar range is derived from the measurements at 0.91 and 0.86 μm, but there is no information about the cloud particle absorption from POLDER data. There is a real gap that can be filled with an instrument such as OSIRIS.

Thanks to the two separated wheels, polarization measurements can be done (or not) at all available wavelength. The nominal measurement configuration is shown on **Table 1**. For instance, no polarization measurements are made for molecular absorption bands (763, 765, 910, 940, 1365 nm).

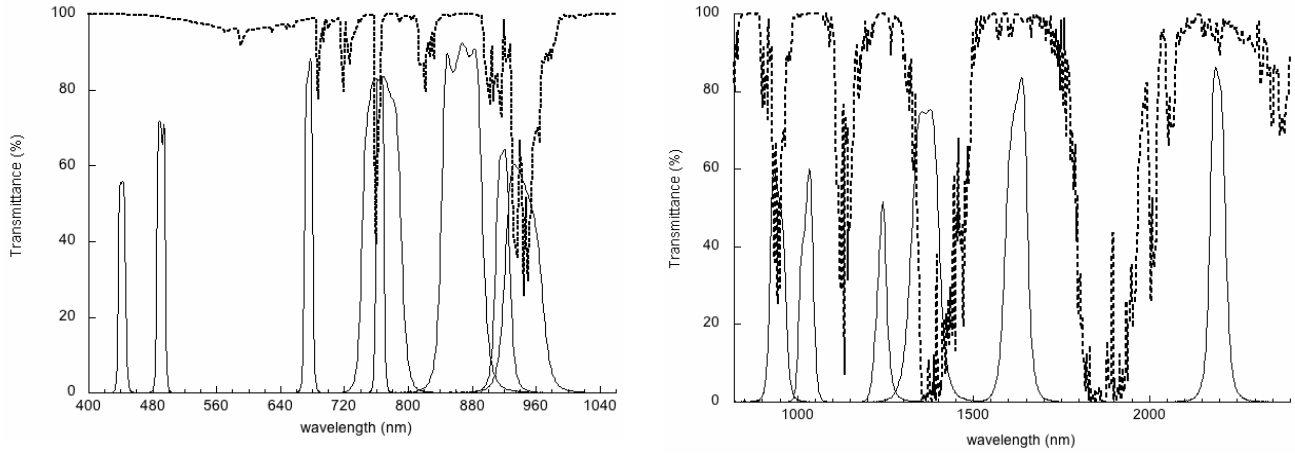

Figure 2. Spectral wavelengths of the VIS-NIR (left) and SWIR (right) part of OSIRIS. The dashed line corresponds to the atmospheric transmittance is plotted

Central Spectral wavelength (nm)	FWHM (nm)	Polarization Measurement	Filter Reference	Filter size (mm)
		VIS-NIR		
440	10	Yes	440FS10-25 (Andover)	25
490	10	Yes	490FS10-25 (Andover)	25
670	12	Yes	NB-0672-012 (Spectrogon)	25.4
763	10	No	100FC37-25 (Andover)	25
765	50	No	500FC47-25 (Andover)	25
865	55	Yes	BP-0865-055 (Spectrogon)	25.4
910	20	No	NB-0910-020 (Spectrogon)	25.4
940	50	No	500FC38-25 (Andover)	25
		SWIR		
940	50	No	500FC38-25 (Andover)	25
1020	40	Yes	BP-1026-040 (Spectrogon)	25.4
1240	35	Yes	NB-1236-035 (Spectrogon)	25.4
1365	80	No	BP-1360-080 (Spectrogon)	25.4
1600	65	Yes	BP-1625-065 (Spectrogon)	25.4
2200	48	Yes	NB-2200-048 (Spectrogon)	25.4

Table 1. List of spectral wavelengths of the visible (VIS-NIR) and shortwave infrared (SWIR) part of OSIRIS instrument.

2.3 Polarization measurements

Polarization measurements are made using POLDER method [40, 41]. For the concerned spectral bands, a polarizer is added to the filters, on the second rotating wheel, in order to assess the degree of linear polarization and the polarization direction. These parameters are derived by combining measurements made with three polarizers shifted by an angle of 60°. The three polarization measurements of a spectral band are successive with a time step of 200 ms between two polarizer positions to which we have to add the integration time that can typically vary from 1 to 110ms (VIS-NIR) and from 1 to 25 ms (SWIR), depending on the observed scene (aerosols, clouds, land surfaces, ocean).

2.4 Optical blocks

Both of the two optics (VIS-NIR and SWIR) are telecentric for the light to cross perpendicularly the interference filters. They are designed to resist to aeronautic conditions (external temperature -65°C and low pressure). **Table 2** shows a comparison of the characteristics of OSIRIS visible and SWIR optics.

	VIS-NIR	SWIR
Focal length	3.6mm	5.2mm
Aperture	F/5.6	F/5
Horizontal Field Of View	+/- 51.1°	+/- 45.5°
Vertical Field Of View	+/- 42.9°	+/- 39.2°
Diagonal Field Of View	+/- 57.15°	+/- 52.5°
Detector size	8.9x6.7mm	9.6x7.7mm
Pixel size	6.45µm*6.45µm	30µm*30µm
Number of pixels	1384*1032	320*256

Table 2. Optical characteristics of OSIRIS lens (VIS-NIR and SWIR)

The VIS-NIR optics (**Figure 3**) has been realized by CERCO. It consists in a wide Field Of View (FOV) telecentric lens. The VIS-NIR optics has a focal lens of 3.6mm, and F/5.6 opening with a diagonal FOV of 114° for a diagonal image of 11mm (rectangular matrix of 8.9*6.7 mm, see section 2.5). At the front, a silica lens protects the optics and reduces thermal effects thanks to the low dilatation coefficient of silica. Then, an aspherical lens reduces the effect of the incidence angle on the entrance pupil area. The total length of the VIS-NIR optics is 139 mm. The FTM is more than 75% on most of the surface image, and > 55% at the edge. The lens distortion (i.e. the difference with the image

formation law: Y=F.Tanθ, F being the focal length and θ the half field angle) is < 8 µm at the edge. Illumination homogeneity is of 90% and decreases for wide field angles. The mean transmission is > 80%. Anti-reflection coating is used to reduce induced polarization (with a 8% maximum at the edge at 865 nm).

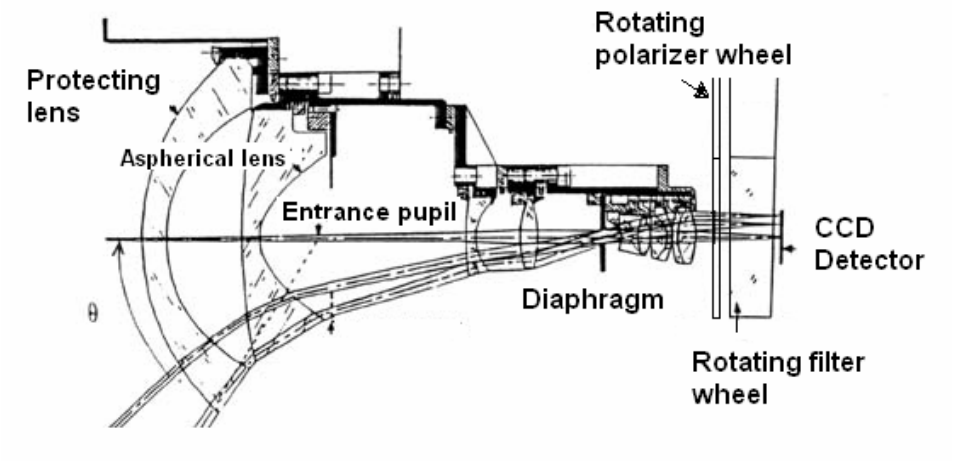

Figure 3. OSIRIS visible lens

The SWIR optics has been designed by SODERN. The length of the optics is 185 mm, with a maximum diameter of 110mm. It has a focal length of 5.2mm with a fixed F/5 opening. It is an optical telecentrical combination of 8 spherical lenses of ZnS and different optical glasses. As for the visible optics, a silica protecting lens is installed at the front. The lack of an aspherical lens induces reduced performances (more distortion, lateral chromatism..) compared to the VIS-NIR. The diagonal field of view is 105° for a diagonal image of 12 mm (rectangular matrix of 9.6*7.7 mm). The lens presents a distortion of about 10% which decreases the ground spatial resolution at the edge of the detector for wide viewing angles. The transmission of the lens is above 65%. Illumination non-uniformity at 1026 nm is 9% and increases up to 40% at 2200nm. The mean FTM is above 76%. Induced polarization is maximum at 1026 nm (15%) and decreases to 5% at 2200nm. Axial chromatism (variation of the position of the focal plane with wavelength) is corrected with glass blades, also used to compensate difference of thickness of the filters.

2.5 Detectors

Both detectors (VIS-NIR and SWIR) are equipped with an anti-blooming system draining away extra charges to do not affect surroundings pixels in case of dynamic range overflow.

The VIS-NIR detector is a Kappa DX2HC thermo-electrically cooled (at 5°C) camera. In fact it is equipped with a Sony ICX285AL progressive scan CCD of 1384*1032 pixels with a pixel size of 6.45x6.45 µm allowing individual readout of the image signals from all pixels. The image diagonal size is of 11 mm (2/3"). The charge handling capacity of this detector is 18000e^-. The output noise is 13 e^- RMS and the SNR is 63 dB. The integration time is programmable from 1 to 110ms. Its spectral range is 400-1000 nm. The frame rate is 9 images/s (binning is possible and increases the frame rate to 50 images/s). It is equipped with an electronic shutter with variable charge storage time.

The SWIR detector is a SOFRADIR IDMS076 [42] detector which includes a 320x256 focal plane array integrated into a metallic dewar and cooled by a four stages thermoelectric cooler. It is composed of a detection module of 320x256 CMT photodiodes arranged in a pitch of 30µm. This module is hybridized on a silicon multiplexed readout circuit. The FPA operating temperature is 197K. It covers the spectral range 900-2500nm. Its charge handling capacity is>1.12 $10^6 e^-$, integration time is programmable, from 100µs to 25ms and its typical readout noise is 250e^-. The pixel SNR is >400, the non-uniformity <5%RMS. At 195K, dark current is 1.1 10^{-14} A/μm^2.

2.6 Operational mode

The camera modules are installed in the optical head box of the instrument as well as the step by step motor control unit of the filter and analyser wheels. The imaging system is controlled by a PIC18F452 micro-controller linked to the external acquisition PC via a serial line. The output video signal format is IEEE1394 12 bits for the visible CCD and parallel 14 bits LVDS for the SWIR detector. SOFRADIR Easylink-01 Digital Proximity Electronic is used to interface the system electronics and the SWIR detector. The PC drives the acquisition and also collects position and attitude data from the Inertial Navigation System, essential to data post-processing. Each channel has its own time stamp and the VIS-NIR and SWIR systems are running freely. The acquisition software allows the user to control the choice of filters and analysers associations as well as the integration time of each channel.

3. IMPLEMENTATION-INSTRUMENT CAPABILITY

3.1 In lab calibration

Calibration process for the visible channels of OSIRIS is very similar to the one previously developed for the POLDER instrument [30, 41]. We mainly provide here details on the calibration results of the SWIR part.

Measurements of the dark current of the SWIR detector have been made. It consists in evaluating the residual signal (or optical "Zero") when a shutter is placed on the polarizer wheel, at the front of the detector. On **Figure 4**, the dark current (in numerical counts NC) is plotted versus the integration time (Ti, in ms) for two 8x8 pixels different zones of the SWIR matrix, in a corner and the second in the middle of the matrix, respectively. These measurements show that the zero values vary as a function of the integration time and can constitute the total part of the signal for integration times above 25ms. It also depends on the pixel position in the matrix and derives as a function of the internal box temperature. Therefore one optical zero is measured for each different integration time used in a complete filter wheel acquisition.

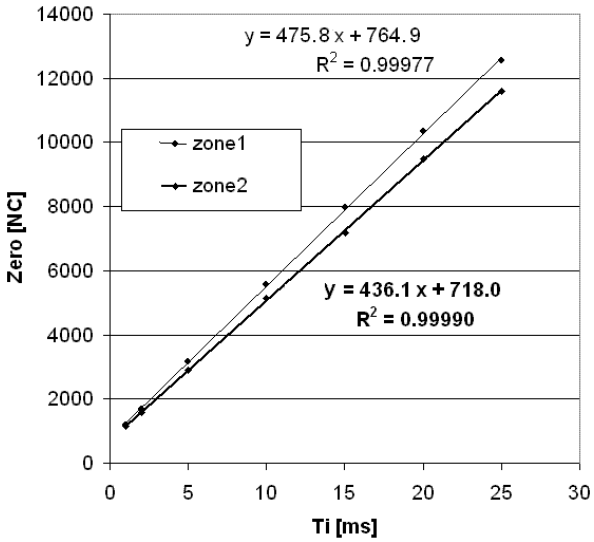

Figure 4. Variation of the dark current in two different zones of the SWIR matrix

To evaluate the linearity of the detectors, we use an integration sphere providing a very stable uniform radiance source. We measure the signal (in numerical counts) corrected from the zero value (referred as S-Z) for varying integration times. **Figure 5** shows for each wavelength, a good linearity of the detectors, in the explored range of integration times (from 1 to 110 ms in the VIS-NIR and 1 to 12ms in the SWIR). A linear interpolation is then applied to bring back measurements made at one integration time to any integration time.

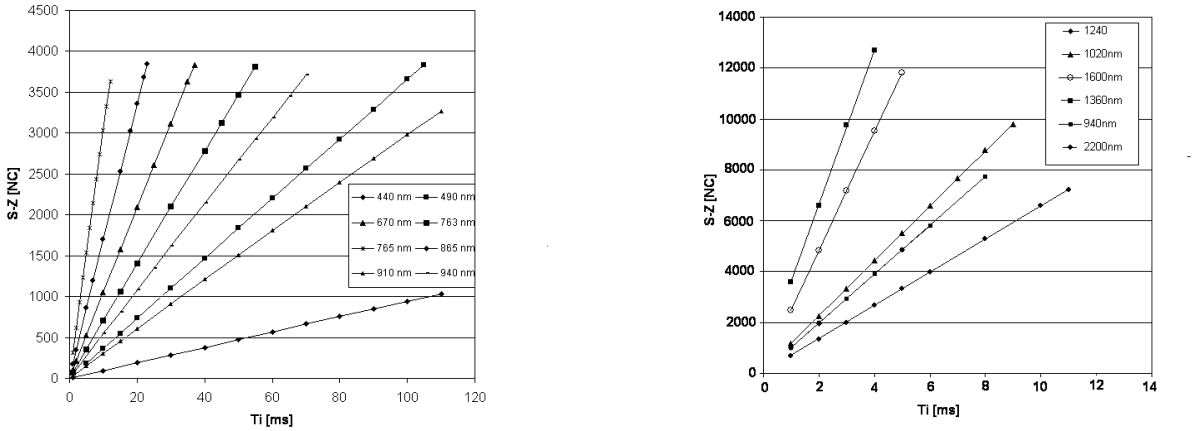

Figure 5. Variation of the signal as a function of the integration time for (left) the 8 VIS-NIR channels and (right) the 6 SWIR channels.

The radiometric calibration in absolute reflectance is derived from secondary standards, using a calibrated integrating sphere (Labsphere or Hoffman). The estimated accuracy of the calibration, directly linked to the uncertainty on the sphere calibration, is below 4% in the visible, 6% in the NIR and lower SWIR wavelengths, 10% at higher wavelengths (from 1240 to 2200nm). For the spectral bands currently associated to polarizers, these calibration coefficients are corrected by determining the rate of signal received by the detector with and without the polarizer.

The polarization calibration is made using a polarizing box. Placed in front of an integrating sphere (delivering natural light), it allows to control the linear polarization rate by tilting two parallel glass blades. The measured polarization rate is compared to the one given by the polarizing box using a linear regression. The obtained fit parameters for each channel are given in **Table 3**. We also give the type of the analyzer used. Results found in the visible and near infrared channels show polarization efficiencies close to 99% except at 865nm where it is close to 70%. They are much lower in the SWIR channel (40% at 2200nm) which reveals a problem that could be caused by the sapphire window at the front of the SWIR detector which could depolarize the input light. This detector will be soon replaced by a new one having an infrasil synthetic glass which will not depolarize the signal. This has to be more investigated. Optics could also be incriminated by inducing polarization (we have seen in section 2.4 that it is of 15% at 1026nm and decrease to 5% at 2200nm according to the manufacturer, which has to be verified).

Wavelength [nm]	slope	intercept	Type of analyser
440	1.0065	0.1731	HN22
490	1.0053	0.3517	HN22
670	1.0085	0.1890	HN22
763	No polarization measurement		
765	No polarization measurement		
865	1.4024	0.4733	HR
910	No polarization measurement		
940 VIS	No polarization measurement		
940 SWIR	No polarization measurement		
1020	1.4293	1.2207	HR
1240	1.9575	-1.9284	HR
1365	No polarization measurement		
1600	2.9522	-1.7454	HR
2200	2.8491	0.8387	HR

Table 3. Polarization calibration coefficients.

To account for optics imperfections (inhomogeneity of the light received on the detector, vignetting…) and for the inter-pixel different responses, we need to inter-calibrate the pixels. OSIRIS has been placed in front of an integration sphere (which provides a stable and uniform radiance source) and the mean resulting image is then normalized by the mean signal measured in the central zone of the matrix. For each wavelength and each pixel, a correction coefficient G_{ij} is then applied to get a uniform image. Results obtained for a horizontal section crossing the center of the image are shown on **Figure 6**. The sharp decrease around pixels #150 and 1190 (in the VIS-NIR, left side) and #20 and 300 (in the SWIR, right side) is caused by the junction section of the half spectralon spheres that compose the calibration sphere. We can note that the manufacturer of the SWIR lens gives an illumination non-uniformity of 9% for 1020nm, increasing to 40% for 2200nm (see section 2.4) which corresponds to our results.

Further analysis of the optical system will include the geometrical characterization of the instrument to account for the distortion, the chromatic aberrations, the determination of the optical axis position and the correction of stray light of the first and second kind.

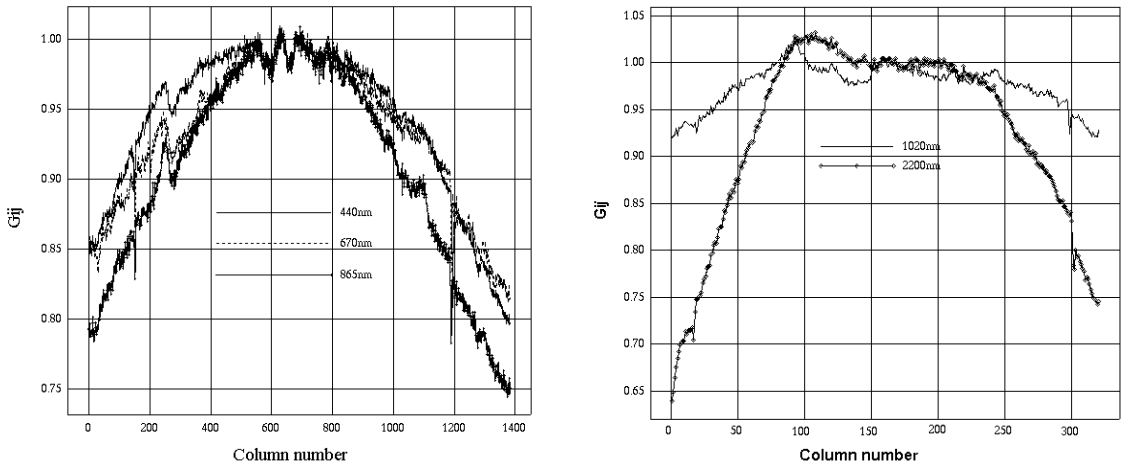

Figure 6. Gij coefficient for a horizontal section, at (left) 440, 670 and 865nm and (right) 1020 and 2200 nm as a function of the pixel column number.

3.2 Aircraft setup and first images

OSIRIS has already been certified for flying on the French Atmospheric Research airplane Dassault Falcon 20. It is a jet aircraft for high troposphere and low stratosphere measurements (ceiling 12km, cruising speed: 150 to 250m/s). After a series of test flights, the first field campaign took place in May 2008 over North-western Europe. A flight was performed on May 21 between Creil (France) to Rotterdam (The Nederland) and Oberpfaffenhofen (Germany). Cloud-free sky was observed between Creil and Rotterdam in the morning. This flight was performed within the frame of the EUCAARI field experiment for studying the long range transport of pollution aerosol over Europe.

In order to increase the number of viewing angles for a same target at the ground, the two lenses are oriented along track, with the SWIR lens at the front, as shown on **Figure 7** (right). When considering all the filters listed in **Table 1**, the time period for the acquisition of a complete VIS-NIR wheel last about 5.5 s (4.7 s for the SWIR). The time between the acquisition of two successive polarizers is about 200 ms. Adding the integration time duration of the 3 filters (from 10 to 80 ms in the VIS-NIR and from 4 to 15 ms in the SWIR, depending on the target characteristics), we have a total duration for a triplet acquisition of 430 to 640 ms which means data have to be registered to take into account the aircraft motion during this time (considering a speed of 200 m/s, the distance covered by the plane between the first image and the last image of a triplet will be of about 100m). The airplane being at a height of about 10km and flying with a speed of 200 to 250m/s, a same target at the ground is seen under about 20 different angles for the visible optical head and 19 for a SWIR image. Taking into account the characteristics of the detector (number, pixel size) and the FOV of both heads

(see **Table 2**), the pixel size at the ground is 18m and 58m respectively for the VIS-NIR and SWIR The swath is about 25x19 km for the visible and 19x15 km for the SWIR for a typical aircraft height of 10km (**Figure 7**).

The data collected on-board consists in the VIS-NIR and SWIR sequence of images and the navigation data from the Inertial Navigation System of the aircraft that are used to co-locate the images in space and time. On **Figure 8,** we show 2 calibrated images acquired at 940 nm in the VIS-NIR and the SWIR over crop surfaces in the North of France. We can observe saturation due to low level cumuli on the right side of the image. The left side corner of the SWIR image is missing due to a shift of the filter wheel during the flight. Inter-calibration of VIS-NIR and SWIR optical system is undergoing and shows a good agreement.

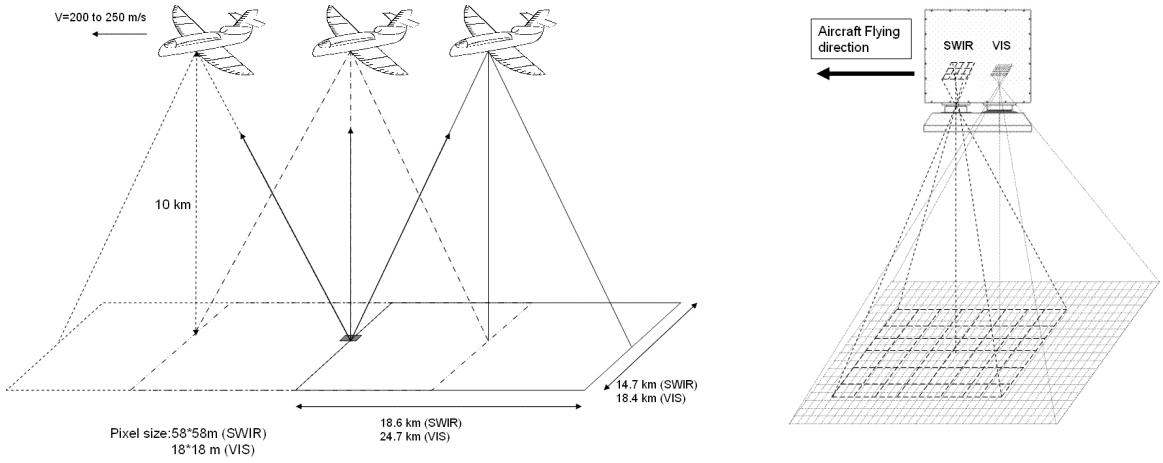

Figure 7. (left) OSIRIS multidirectional viewing principle and swath and (right) orientation of the instrument on the aircraft

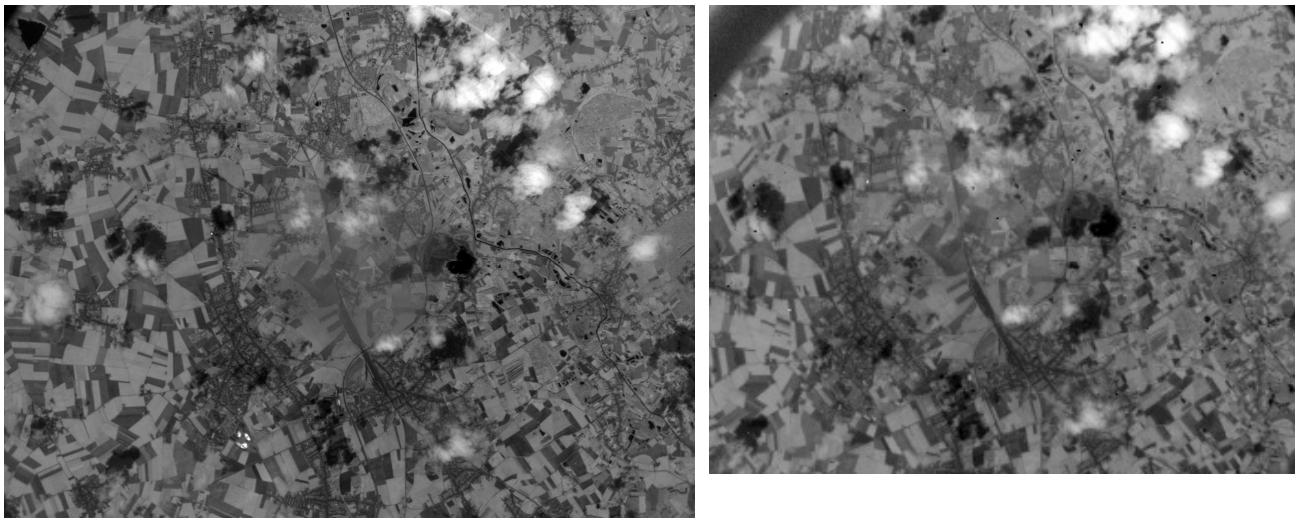

Figure 8. Normalized radiances acquired during EUCAARI flight on May 21, 2008 at 940 nm with the VIS-NIR (left) and at 940 nm with the SWIR (right).

4. CONCLUSION

We have developed a new airborne imaging polarimeter for cloud and aerosol remote sensing. This instrument can measure the linear degree of polarization from 440 nm to 2200 nm in given narrow band channels. We have presented in this paper a detailed description of the instrument and the first characterization of the optical system including the calibration process. The instrument has been tested aboard the French research aircraft Falcon-20 at a nominal altitude of 10km. The comparison of the two common channels of the SWIR and VIS-NIR optical blocks shows encouraging results. Further work is required for the projection and computation of the polarized radiances.

REFERENCES

[1] Forster,P. et al., "Changes in atmospheric constituents and in radiative forcing, in Climate change 2007: The physical basis. Contribution of Working group I to the fourth assessment report of the Intergovernmental panel on climate change", S. Solomon et al. Editors, Cambridge University Press: Cambridge, United Kingdom and New York, NY, USA,(2007).

[2] Cess, R. D. et al., "Intercomparison and interpretation of climate feedback processes in 19 atmospheric general circulation models", J. Geophys. Res., 95, 16601-16610 (1990).

[3] Cess, R.D. et al., "Cloud feedback in atmospheric general circulation models: An update", J. Geophys. Res. 101, 12791-12794 (1996).

[4] Senior, C.A. and Mitchell, J.F.B, "Carbon dioxide and climate: The impact of cloud parameterization", J. Climate 6, 393-418 (1993).

[5] King, M.D., et al., "Remote sensing of tropospheric aerosols from space: past present and future", Bull. Amer. Meteor. Soc. 80(11), 2229-2259 (1999).

[6] Kaufman,Y. J., Tanré, D. and Boucher, O., "A satellite view of aerosols in the climate system", Nature 419, 215-223 (2002).

[7] Tanré, D., Herman, M. and Kaufman, Y. J., "Information on aerosol size distribution contained in solar reflected radiances", J. Geophys. Res. 101, 19043-19060 (1996).

[8] Salomonson, V. V., et al., "MODIS: Advanced facility instrument for studies of the Earth as a system", IEEE Trans. Geosci. Remote Sens. 27, 145-153 (1989).

[9] Tanré, D., et al., "Remote sensing of aerosol properties over oceans using the MODIS/EOS spectral radiances", J. Geophys. Res. 102, 16971-16988 (1997).

[10] Fraser, R. S. and Kaufman, Y. J., "The relative importance of aerosol scattering and absorption in remote sensing", IEEE Trans. Geosci. Remote Sens. 23, 625-633 (1985).

[11] Kaufman, Y. J. and Sendra, C. , "Algorithm for automatic atmospheric corrections to visible and near-IR satellite imagery", Int. J. Remote Sens. 9, 1357-1381 (1988).

[12] Popp, C., et al., "Remote sensing of aerosol optical depth over central Europe from MSG-SEVIRI data and accuracy assessment with ground-based AERONET measurements", J. Geophys. Res. 112,-, (2007).

[13] Bréon, F. M., et al., "Polarized Reflectance of Bare Soils and Vegetation : Measurements and Models", IEEE Trans. Geosci. Remote Sens. 33, 487-499 (1995).

[14] Deuzé, J. L., et al., "Analysis of the POLDER (POLarization and Directionnality of Earth's Reflectances) Airborne Instrument Observations over Land Surfaces", Remote Sens. Environ. 45, 137-154 (1993).

[15] Cairns, B., Travis L. D. and Russel, E. E., "An analysis of polarization: Ground-based upward looking and aircraft/satellite-based downward looking measurements",SPIE,- (1998).

[16] Rondeaux, G. and Herman, M. , "Polarization of light reflected by crop canopies", Remote Sens. Environ., 38, 63-75 (1991).

[17] Nadal, F. and Bréon, F. M., "Parametrisation of surface polarised reflectance derived from POLDER spaceborne measurements", IEEE Trans. Geosci. Remote Sens. 37, 1709-1718 (1999).
[18] Kaufman, Y. J., et al., "Operational remote sensing of tropospheric aerosol over land from EOS moderate resolution imaging spectroradiometer", J. Geophys. Res. 102, 17051-17067 (1997).
[19] Kaufman, Y. J., et al., "The MODIS 2.1-µm channel correlation with visible reflectance for use in remote sensing of aerosol", IEEE Trans. Geosci. Remote Sens. 35, 1286-1298 (1997).
[20] Remer, L. A., et al., "The MODIS Aerosol algorithm, Products, and validation", J. Atmos. Sci. 62, 947-973 (2005).
[21] Waquet, F., et al., "Aerosol retrieval over land using a multiband polarimeter and comparison with path radiance method", J. Geophys. Res. 112,- (2007).
[22] de Almeida Castanho, A.D., et al., "Analysis of visible/SWIR surface reflectances ratios for aerosol retrievals from satellite in Mexico City urban area", Atmos. Chem. Phys. 7, 5467-5477 (2007).
[23] Deschamps, P.Y., et al., "The POLDER mission: Instrument characteristics and scientific objectives", IEEE Trans. Geosci. Remote Sens. 32, 598-615 (1994).
[24] Herman, M., et al., "Aerosol remote sensing from POLDER/ADEOS over the ocean: Improved retrieval using a nonspherical particle model", J. Geophys. Res. 110,- (2005).
[25] Deuzé, J.-L., et al., "Remote sensing of aerosols over land surfaces from POLDER-ADEOS-1 polarized measurements", J. Geophys. Res. 106, 4913-4926 (2001).
[26] Dubovik, O., et al., "Non- spherical aerosol retrieval method employing light scattering by spheroids", Geophys. Res. Lett. 29,- (2002).
[27] Kahn, R., Banerjee, P. and McDonald, D., "Sensitivity of multiangle imaging to natural mixtures of aerosols over ocean", J. Geophys. Res. 106, 18219-18238 (2001).
[28] Mishchenko, M., et al., "Accurate monitoring of terrestrial aerosols and total solar irradiance: introducing the GLORY mission", Bull. of Amer. Meteor. Soc. 88, 677-691 (2007).
[29] Leroy, M., et al., "Retrieval of atmospheric properties and surface bidirectionnal reflectances over land from POLDER/ADEOS", J. Geophys. Res. 102, 17023-17037 (1997).
[30] Hagolle, O., et al., "Results of POLDER in-flight absolute calibration", IEEE Trans. Geosci. Remote Sens. 37, 1550-1566 (1999).
[31] Vanbauce, C., et al., "Apparent pressure derived from ADEOS-POLDER observations in the oxygen A-band over ocean", Geophys. Res. Lett. 25, 3159-3162 (1998).
[32] Dubuisson, P., et al., "Estimation of aerosol altitude from reflectance ratio measurements in the O2 A-band", Remote Sens. Environ. (submitted),- (2008).
[33] Dubuisson, P., et al., "Water vapor retrieval over ocean using near-infrared radiometry", J. Geophys. Res. 109,- (2004).
[34] Vesperini, M., Bréon, F.-M. and Tanré, D., "Atmospheric water vapor content from spaceborne POLDER measurements", IEEE Trans. Geosci. Remote Sens. 37, 1613-1619 (1999).
[35] Gao, B.C., Goetz, A.F.H. and Wiscombe, W.J., "Cirrus cloud detection from airborne imaging spectrometer data using the 1.375µm water vapor band", Geophys. Res Lett. 260, 523-526 (1992).
[36] King, M.D., et al., "Remote sensing of cloud, aerosol, and water vapor properties from the moderate resolution imaging spectrometer (MODIS)", IEEE Trans. Geosci. Remote Sens. 30, 2-27 (1992).
[37] Nakajima, T. and King, M. D., "Determination of the optical thickness and effective raidus of clouds from reflected solar radtiation measurements. Part I: Theory", J. Aerosol Sci. 47, 1878-1893 (1990).
[38] Twomey, S. and Cocks, T., "Remote sensing of cloud parameters from spectral reflectance measurements in the near-infrared", Beitr. Phys. Atmos. 62, 172-179 (1989).
[39] Coffen, D.L. and Hansen, J., H., "Polarization studies of planetary atmospheres, in Planets, Stars and Nebulae", T. Gehrels Editor,- (1974).
[40] Hagolle, O., et al., "POLDER Level 1 processing algorithm. in Algorithms for multispectral and hyperspectral imagery II", SPIE (Orlando FL),-(1996).
[41] Goloub, P., et al., "Analysis of the POLDER polarization measurements performed over cloud covers", IEEE Trans. Geosci. Remote Sens. 32, 78-88 (1994).
[42] Chorier, P. and Tribollet, P., M., "High performance HgCdTe SWIR detectors development at Sofradir in Infrared technology and applications", SPIE XXVII (Orlando FL),- (2001).